J Mol Model (2014) 20:2091
DOI 10.1007/s00894-014-2091-1

ORIGINAL PAPER

A DFT study of permanganate oxidation of toluene and its *ortho*-nitroderivatives

Paweł Adamczyk · Reto S. Wijker ·
Thomas B. Hofstetter · Piotr Paneth

Received: 10 September 2013 / Accepted: 20 November 2013 / Published online: 14 February 2014

Abstract Calculations of alternative oxidation pathways of toluene and its *ortho*-substituted nitro derivatives by permanganate anion have been performed. The competition between methyl group and ring oxidation has been addressed. Acceptable results have been obtained using IEFPCM/B3LYP/6-31+G(d,p) calculations with zero-point (ZPC) and thermal corrections, as validated by comparison with the experimental data. It has been shown that ring oxidation reactions proceed via relatively early transition states that become quite unsymmetrical for reactions involving *ortho*-nitrosubstituted derivatives. Transition states for the hydrogen atom abstraction reactions, on the other hand, are late. All favored reactions are characterized by the Gibbs free energy of activation, $\Delta G^{\neq}$, of about 25 kcal mol^{-1}. Methyl group oxidations are exothermic by about 20 kcal mol^{-1} while ring oxidations are around thermoneutrality.

Keywords Permanganate · B3LYP · DFT · HOMA · Nitroaromatic pollutants · Toluene

Introduction

Anthropogenic influence on the natural environment results in the presence of a wide range of aromatic pollutants in soil, sediments, as well as surface- and groundwaters since aromatic compounds are widely used by industries but also they are a component of gasoline and oils [1, 2]. These compounds are of high toxicity, stability and ability of bioaccumulation and depending on the component of the ecosystem in which they are present, they may undergo a transition through the various abiotic or biological processes. In addition, products of such degradation reactions may also pose a significant environmental hazard [1, 2]. In recent years mechanisms of these processes have been intensively studied in search of the best methods for removal of aromatic compounds from the environment.

It has been shown than oxidative degradation of many of these contaminants, both biotic and abiotic, may proceed via two competitive pathways: aromatic ring oxidation and methyl group oxidation [3, 4]. In environmental field studies compound specific isotope analysis (CSIA) is increasingly used for quantitative estimates of ongoing degradation processes. In the case of polynitroaromatic pollutants, such as mono-, dinitrotoluenes, typical analysis of carbon and hydrogen isotope fractionation combined with reaction progress is difficult to establish as outlined in a companion paper [5]. Thus a more fundamental understanding of possible oxidation pathways is essential not only for the selection of an appropriate treatment but also for improvement of CSIA-based accessing of degradation processes of nitroaromatic compounds [6]. As permanganate, the most popular oxidant for the in situ chemical oxidation, is capable of oxidizing both aromatic ring and aliphatic chains [5, 7] we have used it as a model oxidant for our studies of oxidative degradation of common aromatic pollutants.

The mechanism of toluene oxidation by permanganate has been the subject of detailed experimental [8–12] and theoretical studies [13]. However degradation of nitroaromatic compounds by permanganate was not studied to an extent that

P. Adamczyk · P. Paneth (✉)
Institute of Applied Radiation Chemistry, Faculty of Chemistry, Lodz University of Technology, Zeromskiego 116, 90-924 Lodz, Poland
e-mail: paneth@p.lodz.pl

R. S. Wijker · T. B. Hofstetter (✉)
Eawag, Swiss Federal Institute of Aquatic Science and Technology, 8600 Dübendorf, Switzerland
e-mail: thomas.hofstetter@eawag.ch

would allow one to assess the relative shares of oxidation at the alkyl vs. aryl moieties. Herein we present detailed theoretical study of the rate-determining step of permanganate oxidation of three aromatic pollutants; toluene and its two nitro derivatives, 2-nitrotoluene and 2,6-dinitrotoluene, which were chosen due to their environmental importance.

Methodology

Two DFT functionals M05-2X [14, 15] and B3LYP [16–18] expressed in 6-31+G(d,p) [19–23] basis set with aqueous solution modeled by IEFPCM continuum solvent model [24] utilizing the UFF [25] atom radii have been used. These levels of theory have been chosen based on our previous studies [26, 27]. Energy calculations for the selected stationary points have been carried out using the same functionals in combination with a significantly larger basis set, aug-cc-pVTZ [28]. Except for the hydrogen abstraction from the methyl group where unrestricted open shell method [29] was applied, singlet state using default restricted closed shell method was used. All quantum-mechanical calculations were performed using Gaussian package G09 rev. A.02 [30] with default convergence criteria. Vibrational analysis was performed not only to confirm that obtained optimized geometries indeed correspond to stationary points (either local minimum or first order saddle point) on the potential energy surfaces but also to evaluate contributions of vibrational motions to thermochemistry calculations. Merz-Singh-Kollman population analysis [31, 32] has been performed for all obtained stationary points. Transition states of modeled reactions have been located using Berny algorithm [33, 34]. All reaction pathways have been investigated using intrinsic reaction coordinate (IRC) [35] protocol in which end points have been subsequently optimized to either reactants or products. Calculations of reaction pathways probabilities, were based on Eyring-Polanyi equation [36–38]. The influence of the tunneling was tested using Wigner correction [39]. Aromaticity indexes have been calculated for all structures using reformulated harmonic oscillator model of aromaticity (HOMA) [40, 41]. Bond orders were calculated using Pauling equation [42].

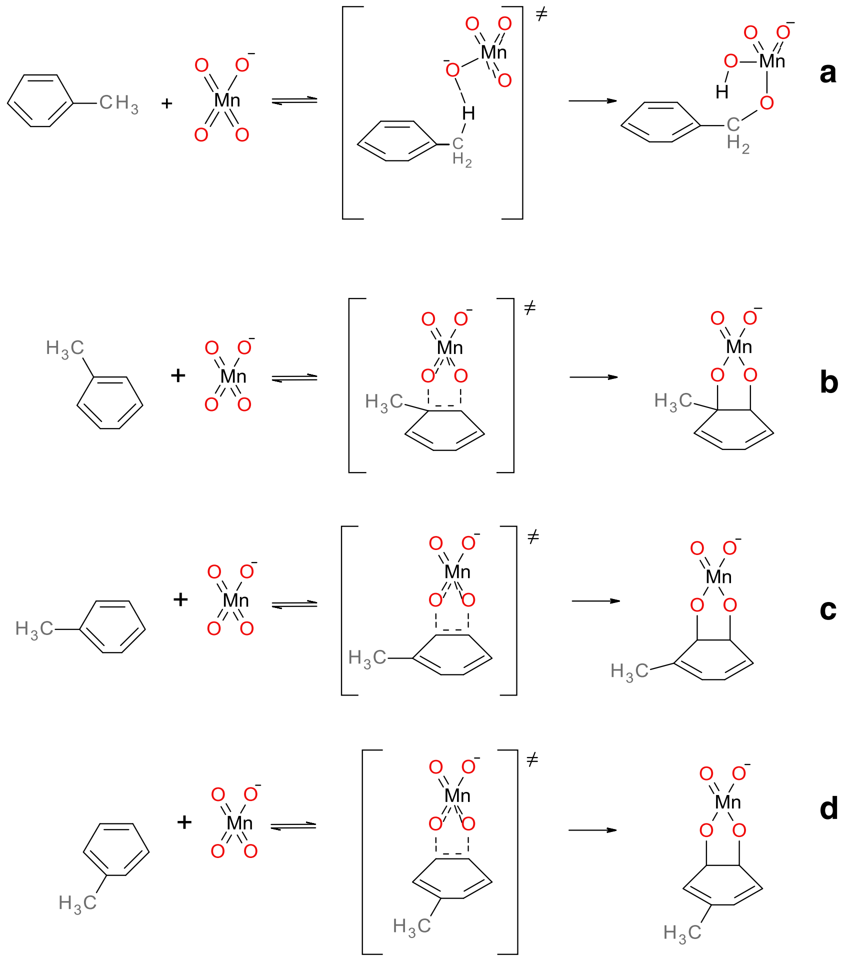

Fig. 1 Possible reactions of toluene and with permanganate anion at positions: **a** C_m, **b** C_1-C_2, **c** C_2-C_3, **d** C_3-C_4

Results and discussion

Toluene

Environmental studies of the oxidation of toluene nitroderivatives by permanganate anion show that hydrogen atom abstraction from the methyl group competes with the ring oxidation. The first, rate-determining step in the case of hydrogen abstraction is formation of the benzyl radical while in the case of the ring oxidation it is formation of the adduct. We have considered a simple model for these processes, i.e., reactions of permanganate anion with toluene using previously employed theory level [26, 27]. Three different regioselective attacks of permanganate anion on the aromatic ring are possible here as presented in Fig. 1. Results collected in Table 1 show that Gibbs free energy of activation ($\Delta G^{\neq}$) for aromatic ring oxidation is smaller than the one for the hydrogen atom abstraction from methyl group. The percentage contributions of alternative pathways of toluene oxidation, %F, (calculated from ratios of Gibbs free energies of activation) do not, however, agree with the experimental results [5], which indicate that the predominant pathway of this reaction is hydrogen atom abstraction from the methyl group. These results question the applicability of the theory level used previously [26, 27] to the present systems. We have, therefore, started our studies by identifying a theory level that properly describes the competition between the pathways a – d presented in Fig. 1.

Since the percentage contribution of the competing pathways results from the energetic barriers, we have extended IEFPCM/M05-2X/6-31+G(d,p) by including ZPC and thermal corrections and by calculating energies using larger basis set. As can be seen from the results listed in Table 1, only after including all of these correction does one obtain the agreement between experiment and theory. When, however, B3LYP functional has been used instead of M05-2X, even the results obtained with smaller basis set became acceptable when ZPC and thermal corrections were included (see the last three entries in Table 1). Furthermore, inclusion of tunneling correction (values reported in parenthesis in the last column) did not affect the results significantly. Therefore B3LYP/6-31+

Table 1 Activation Gibbs free energies, exothermicity and contribution of alternative pathways (%F) of oxidation of toluene by permanganate anion at several different theory levels (all with IEFPCM)

Attack	$\Delta G^{\neq}$ [kcal mol^{-1}]	ΔG_R [kcal mol^{-1}]	% F
M05-2X/6-31+G(d,p)			
C_m	25.0	−71.9	0.0 (0.0)
C_1-C_2[a]	21.0	−53.9	10.4 (10.4)
C_2-C_3	19.7	−54.2	86.1 (86.1)
C_3-C_4	21.6	−52.4	3.5 (3.5)
M05-2X/6-31+G(d,p) with ZPC and thermal corrections			
C_m	22.2	−66.6	25.6
C_1-C_2	22.6	−48.4	12.8
C_2-C_3	21.8	−48.1	48.2
C_3-C_4	22.6	−47.0	13.3
M05-2X/aug-cc-pVTZ//M05-2X/6-31+G(d,p) with ZPC and thermal corrections			
C_m	18.3	−70.2	99.8
C_1-C_2	22.5	−50.2	0.1
C_2-C_3	22.7	−50.3	0.1
C_3-C_4	26.1	−49.2	0.0
B3LYP/6-31+G(d,p)			
C_m	25.9	−25.9	13.1 (16.5)
C_1-C_2	26.1	−5.8	10.2 (9.8)
C_2-C_3	25.2	−6.8	43.6 (41.9)
C_3-C_4	25.4	−6.4	33.1 (31.8)
B3LYP/6-31+G(d,p) with ZPC and thermal corrections			
C_m	27.2	−20.2	99.7
C_1-C_2	32.2	2.4	0.1
C_2-C_3	30.8	0.9	0.2
C_3-C_4	33.3	3.4	0.0
B3LYP/aug-cc-pVTZ//B3LYP/6-31+G(d,p) with ZPC and thermal corrections			
C_m	24.4	−21.0	99.9
C_1-C_2	33.3	4.0	0.0
C_2-C_3	32.0	2.6	0.1
C_3-C_4	34.6	5.0	0.0
Experimental[5]			
C_m			100
Ring oxidation			0

[a] For atom numbering see Fig. 2

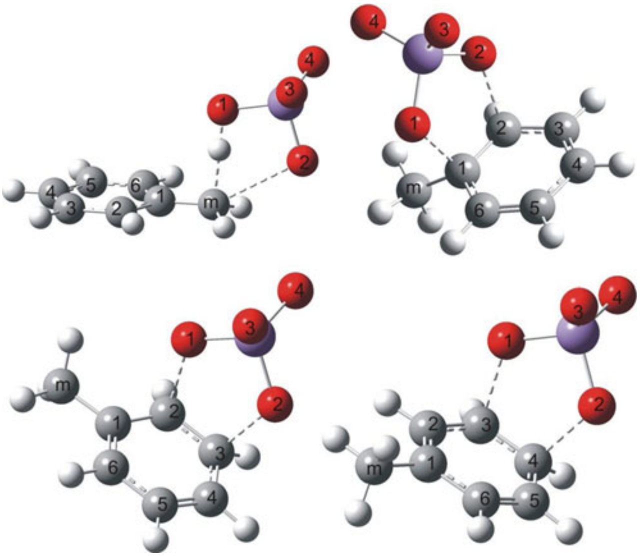

Fig. 2 Optimized structures of transition states of modeled oxidation reactions of toluene with permanganate anion at positions (from *upper, left*): C_m, C_1-C_2, C_2-C_3, and C_3-C_4

G(d,p) with ZPC and thermal corrections has been used in the present studies.

Optimized structures of the transition states corresponding to alternative pathways of toluene oxidation by permanganate together with atom numbering used are shown in Fig. 2. In all ring oxidation cases, we have observed formation of the C-O-Mn-O-C ring, which is almost perpendicular to the aromatic ring surface. In the case of methyl group oxidation, the atoms H-O-Mn-O-C form a similar pseudo-cyclic structure. No bridging structures of transition states corresponding to C_1-C_3, C_1-C_4 attacks or combining ring carbon with methyl group carbon attack have been observed; all these initial structures converged to one of those presented in Fig. 2.

Geometric results are presented in Table 2. In all reactions involving ring oxidation, similar products differing only in the position of attack, are obtained. Corresponding changes of bond distances are also almost identical in all three cases. The same is true for valence angles despite the fact that initial values differ significantly. These reactions proceed analogically to benzene oxidation [27] however transition state structures are not symmetric due to steric hindrance caused by the methyl group. In the transition state of toluene oxidation at the C_1-C_2 bond these distances are different and larger than in other cases; C_1-O_1 bond length equals to 1.98 Å and C_2-O_2 is 1.96 Å, corresponding to bond orders of 0.22 and 0.23, respectively. Elongation of these bonds is a consequence of the steric hindrance exerted by the methyl group. In reactions in which the attack occurs at C_2-C_3 and C_3-C_4 the corresponding values are 1.94 Å and 1.95 Å (bond order of about 0.24) and 1.97 Å (bond orders of 0.22), respectively. Interestingly, the above bond orders for toluene oxidation do not correlate with the barriers as one would expect a slightly earlier transition state for the reaction with lowest barrier. Dihedral angle Φ, defined as C-C-O-Mn, varies for all considered reactions indicating that permanganate anion rotates over the aromatic ring. Interestingly, in the case of both C_2-C_3 and C_3-C_4 oxidation, MnO_4^- rotates in one direction, stops at the transition state (dihedral angles are almost 0), and then rotates back but in the case of C_1-C_2 attack rotation is in one direction only which again may be ascribed to the presence of steric hindrance.

We have carried out calculations of HOMA indices to compare how addition at different positions of the ring influences the aromaticity. Indices collected in Tables 2 and 3

Table 2 Selected geometric parameters (d – distances in Å, α,*Φ* – angles in °) and HOMA aromaticity indexes of modeled oxidation processes of toluene with permanganate ions (R – reactants, TS – transition states, P – products) at IEFPCM/B3LYP/6-31+G(d,p) theory level

Parameter	*R*	*TS*	*P*	Parameter	*R*	*TS*	*P*
Toluene C_m attack				Toluene C_1-C_2 attack			
d_{Cm-H}	1.098	1.521	2.448	d_{C1-C2}	1.403	1.451	1.552
d_{H-O1}	2.583	1.103	0.969	d_{C1-O1}	4.430	1.978	1.450
d_{Cm-O2}	4.245	2.726	1.414	d_{C2-O2}	4.564	1.957	1.435
d_{O1-Mn}	1.600	1.703	1.819	d_{O1-Mn}	1.600	1.658	1.804
d_{O2-Mn}	1.600	1.629	1.822	d_{O2-Mn}	1.600	1.661	1.806
$\alpha_{O1-H-Cm}$	169.5	179.3	116.8	$\alpha_{O1-C1-C2}$	109.0	103.9	106.7
$\alpha_{H-Cm-O2}$	35.5	54.6	80.2	$\alpha_{C1-C2-O2}$	86.7	106.6	107.9
$\alpha_{Cm-O2-Mn}$	94.3	103.8	126.4	$\alpha_{C2-O2-Mn}$	100.4	115.5	115.0
$\alpha_{O2-Mn-O1}$	109.4	95.5	97.9	$\alpha_{O2-Mn-O1}$	109.5	97.4	87.8
$\alpha_{Mn-O1-H}$	117.4	105.4	112.1	$\alpha_{Mn-O1-C1}$	94.8	116.1	115.3
$\Phi_{C1-Cm-O2-Mn}$	−89.1	3.3	−82.3	$\Phi_{C1-Cm-O2-Mn}$	29.5	−5.6	−23.7
HOMA	0.958	0.909	0.962	*HOMA*	0.959	0.459	−1.890
Toluene C_2-C_3 attack				Toluene C_3-C_4 attack			
d_{C2-C3}	1.398	1.444	1.537	d_{C3-C4}	1.398	1.444	1.538
d_{C2-O1}	4.589	1.942	1.443	d_{C3-O1}	4.730	1.969	1.437
d_{C3-O2}	4.936	1.968	1.435	d_{C4-O2}	4.586	1.945	1.443
d_{O1-Mn}	1.600	1.662	1.807	d_{O1-Mn}	1.600	1.661	1.808
d_{O2-Mn}	1.600	1.660	1.810	d_{O2-Mn}	1.600	1.662	1.807
$\alpha_{O1-C2-C3}$	102.4	105.8	107.4	$\alpha_{O1-C3-C4}$	78.1	105.0	107.3
$\alpha_{C2-C3-O2}$	92.1	105.4	107.1	$\alpha_{C3-C4-O2}$	115.0	106.2	107.9
$\alpha_{C3-O2-Mn}$	97.3	115.3	114.3	$\alpha_{C4-O2-Mn}$	110.0	115.8	113.9
$\alpha_{O2-Mn-O1}$	109.5	97.4	87.9	$\alpha_{O2-Mn-O1}$	109.4	97.4	80.0
$\alpha_{Mn-O1-C2}$	106.4	116.1	113.7	$\alpha_{Mn-O1-C3}$	123.4	115.5	114.8
$\Phi_{C1-Cm-O2-Mn}$	34.1	1.4	25.9	$\Phi_{C1-Cm-O2-Mn}$	−28.9	0.1	−25.2
HOMA	0.958	0.485	−1.722	*HOMA*	0.958	0.490	−1.701

Table 3 Bond lengths in aromatic rings (in Å) for HOMA analysis of modeled oxidation processes of toluene with permanganate ions (R – reactants, TS – transition states, P – products) at IEFPCM/B3LYP/6-31+G(d,p) theory level

Parameter	*R*	*TS*	*P*	Parameter	*R*	*TS*	*P*
Toluene C_m attack				Toluene C_1-C_2 attack			
C_1-C_2	1.405	1.417	1.403	C_1-C_2	1.403	1.451	1.552
C_2-C_3	1.398	1.393	1.398	C_2-C_3	1.399	1.438	1.508
C_3-C_4	1.399	1.402	1.399	C_3-C_4	1.398	1.369	1.344
C_4-C_5	1.398	1.402	1.398	C_4-C_5	1.399	1.434	1.466
C_5-C_6	1.399	1.393	1.399	C_5-C_6	1.398	1.368	1.345
C_1-C_6	1.404	1.417	1.403	C_1-C_6	1.405	1.445	1.515
HOMA	0.958	0.909	0.962	*HOMA*	0.959	0.459	−1.890
EN	0.040	0.066	0.037	*EN*	0.039	0.224	1.157
GEO	0.002	0.025	0.001	*GEO*	0.002	0.317	1.733
Toluene C_2-C_3 attack				Toluene C_3-C_4 attack			
C_1-C_2	1.404	1.449	1.519	C_1-C_2	1.404	1.373	1.347
C_2-C_3	1.398	1.444	1.537	C_2-C_3	1.399	1.438	1.509
C_3-C_4	1.399	1.437	1.508	C_3-C_4	1.398	1.444	1.538
C_4-C_5	1.399	1.369	1.345	C_4-C_5	1.399	1.440	1.509
C_5-C_6	1.399	1.434	1.467	C_5-C_6	1.398	1.368	1.345
C_1-C_6	1.404	1.372	1.349	C_1-C_6	1.405	1.442	1.475
HOMA	0.958	0.485	−1.722	*HOMA*	0.958	0.490	−1.701
EN	0.040	0.224	1.128	*EN*	0.040	0.224	1.117
GEO	0.002	0.291	1.594	*GEO*	0.002	0.286	1.584

indicate that dearomatization during all toluene ring oxidation reactions increases as the attack occurs closer to the methyl group. Interestingly, this trend is opposite to the one that could be expected from the C-O bond lengths in the corresponding transition state structures; the shortest being observed for C_2-C_3 (average of 1.55 Å) and the longest for C_1-C_2 attack (average of 1.97 Å). This result of the steric hindrance exerted by the neighboring methyl group illustrates how subtle the balance is between different factors influencing reactivity in the opposite directions.

The above differences regarding the reaction advancement in the transition state gathered from electronic and geometric data were further investigated by performing Merz-Singh-Kollman population analysis (see Table 4). The analysis revealed that initial charges in the reactant complex with orientation for the attack at the C_1-C_2 bond are 0.38 a.u. for C_1 and

Table 4 Charge distribution based on Merz-Singh-Kollman population analysis of selected atoms in modeled oxidation processes of toluene with permanganate ions (R – reactants, TS – transition states, P – products) at IEFPCM/B3LYP/6-31+G(d,p) theory level

Parameter	*R*	*TS*	*P*	Parameter	*R*	*TS*	*P*
Toluene C_m				Toluene C_1-C_2 attack			
H	0.202	0.435	0.396	C_1	0.383	0.381	0.782
C_m	−0.628	−0.782	0.196	C_2	−0.324	0.246	0.638
O_1	−0.543	−0.708	−0.867	O_1	−0.546	−0.567	−0.721
O_2	−0.539	−0.632	−0.677	O_2	−0.546	−0.572	−0.764
Mn	1.163	1.219	1.244	*Mn*	1.192	1.172	1.152
O_3	−0.542	−0.619	−0.672	O_3	−0.553	−0.646	−0.659
O_4	−0.544	−0.619	−0.662	O_4	−0.551	−0.668	−0.669
Toluene C_2-C_3 attack				Toluene C_3-C_4 attack			
C_2	−0.320	−0.067	0.401	C_3	−0.105	0.213	0.347
C_3	−0.107	0.220	0.327	C_4	−0.177	−0.054	0.67
O_1	−0.543	−0.485	−0.635	O_1	−0.555	−0.544	−0.675
O_2	−0.546	−0.519	−0.671	O_2	−0.555	−0.524	−0.680
Mn	1.183	1.110	1.150	*Mn*	1.226	1.176	1.108
O_3	−0.543	−0.636	−0.660	O_3	−0.560	−0.653	−0.650
O_4	−0.552	−0.663	−0.671	O_4	−0.559	−0.675	−0.661

−0.32 a.u. at C_2. In the transition state the charge on C_1 remains unchanged while that on C_2 becomes positive (0.25 a.u.). In the other two reactions these charges systematically and simultaneously increase. In all cases attacked carbons become positively charged in product followed by increasing negative charge on both attacking oxygen atoms and reduction of positive charge on manganese atom.

In the reaction of hydrogen atom abstraction one of the oxygen atoms attacks the hydrogen atom of methyl group while another oxygen atoms moves in the direction of the methyl carbon (and in fact, in the subsequent step the C_m-O bond is formed). The pseudo-cyclic H-O-Mn-O-C structure is nearly perpendicular to the aromatic ring. The geometry of this part of the transition state structure is similar to the one obtained with higher basis set [13] although breaking the toluene C-H bond at IEFPCM/B3LYP/6-31+G(d,p) has the length of about 1.52 Å (bond order of 0.30) while it is 1.67 Å in the case of B3LYP/6-311++G(d,p) while forming O-H bond is about 1.1 Å (bond order of 0.68) in the case of IEFPCM/B3LYP/6-31+G(d,p) and 1.05 Å in the case of higher basis set. A small difference is also observed in the forming C-O bond; 2.73 Å in the case of smaller basis set (bond order of 0.02) and 2.70 Å in the case of higher. Evolution of the dihedral angle throughout oxidation of toluene is quite interesting. These values change from −89.1° for reactants through 3.3° at the transition state to −82.3° for products.

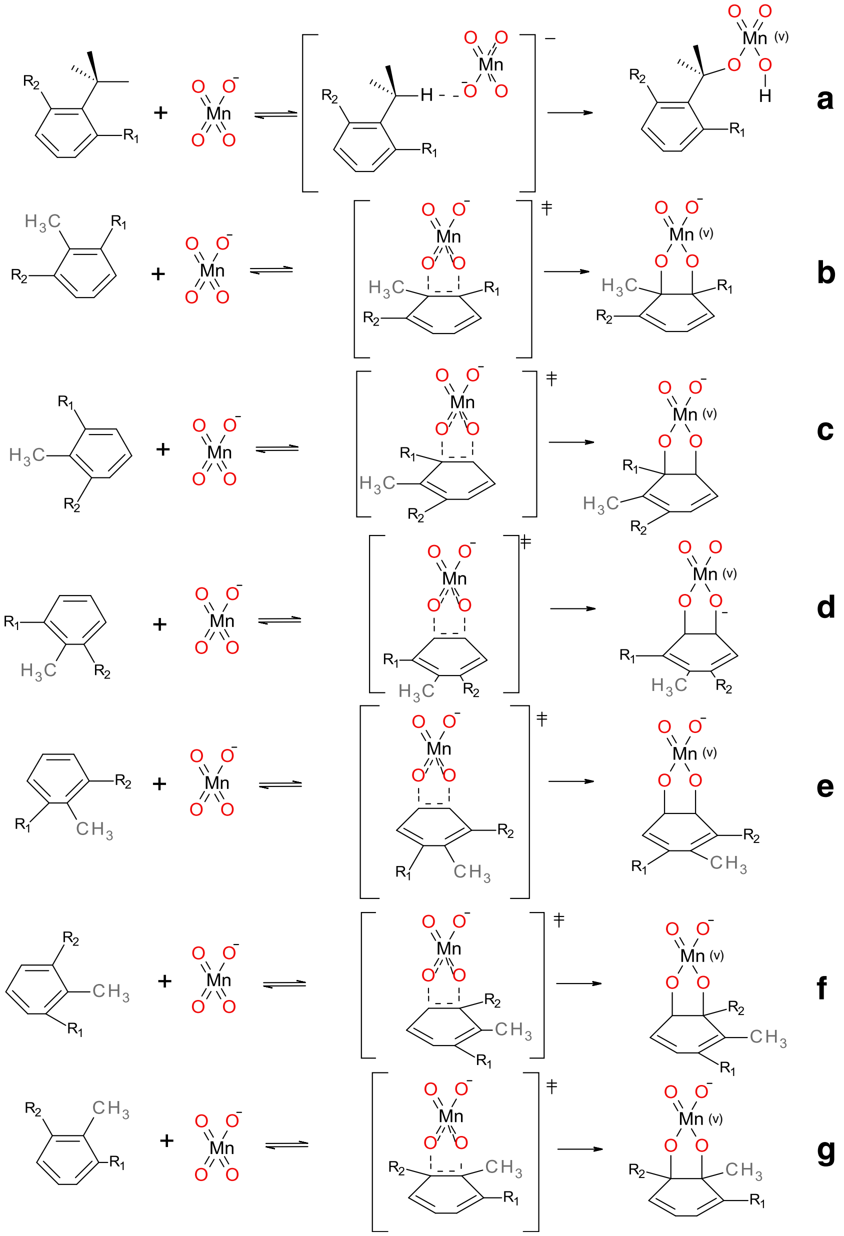

Fig. 3 Modeled oxidation reactions of 2-nitrotoluene (R_1= NO_2, R_2=H) and 2,6-dinitrotoluene (R_1, R_2=NO_2) with permanganate at positions: **a** C_m, **b** C_1-C_2, **c** C_2-C_3, **d** C_3-C_4, **e** C_4-C_5, **f** C_5-C_6, **g** C_1-C_6

Table 5 Activation Gibbs free energies, exothermicity, contribution of alternative pathways and comparison of methyl group vs. ring oxidation with experimental data in oxidation reactions of 2-nitrotoluene and 2,6-dinitrotoluene by permanganate anion

Attack	$\Delta G^{\neq}$ [kcal mol^{-1}]	ΔG_R [kcal mol^{-1}]	% F	% F_{DFT}/% F_{exp}[5]
2-nitrotoluene				
C_m	25.8	−19.1	93.1	93/87
C_1-C_2	29.9	−5.0	0.1	7/13
C_2-C_3	28.5	−7.7	1.0	
C_3-C_4	27.9	−2.7	3.2	
C_4-C_5	28.9	0.2	0.6	
C_5-C_6	28.2	−0.7	1.8	
C_1-C_6	29.4	−0.4	0.2	
2,6-dinitrotoluene				
C_m	24.2	−20.3	67.6	68/58
C_1-C_2	28.0	−8.3	0.1	32/42
C_2-C_3	26.1	−11.0	2.5	
C_3-C_4	24.7	−2.2	29.8	

Analysis of HOMA indices for the methyl group oxidation is also interesting; temporary lowering of aromaticity is observed in the transition state. Analysis of HOMA factors indicate that in this case bond elongation term (EN) is responsible for the change, as opposite to the ring oxidation reactions where it was caused by the bond alternation term (GEO). Population analysis reveals that in the case of methyl group oxidation environment has lower influence on the charge distribution then in the case of aromatic ring oxidation. The attacked carbon atoms become more negatively charged in the transition state (change of 0.15 a.u.) but in the products they are positively charged. Positive charge located initially on the abstracted hydrogen atom (about 0.20 a.u.) increases in the transition state (about 0.43 a.u.) and decreases in products (about 0.40 a.u.). These results do not support earlier suggestions of the hydride transfer in the toluene oxidation by permanganate [10].

2-Nitro- and 2,6-dinitrotoluene

We have selected these two compounds as models because of the extreme differences in relative contributions of alternative oxidation pathways observed for them experimentally. While in the case of symmetrically substituted dinitroderivative alternative pathways are similar to those found for toluene the situation is more complicated in the case of monosubstitution since all six possible ring oxidation processes lead to different products; schematic representation of all

Table 6 Selected geometric parameters (d – distances in Å, α,Φ – angles in °) of modeled oxidation processes of 2,6-dinitrotoluene with permanganate ions (R – reactants, TS – transition states, P – products) at IEFPCM/B3LYP/6-31+G(d,p) theory level

Parameter	*R*	*TS*	*P*	Parameter	*R*	*TS*	*P*
2,6-dinitrotoluene C_m attack				2,6-dinitrotoluene C_1-C_2 attack			
d_{Cm-H}	1.096	1.593	2.863	d_{C1-C2}	1.409	1.475	1.582
d_{m-O1}	2.434	1.077	0.966	d_{C1-O1}	4.056	1.711	1.418
d_{Cm-O2}	3.828	2.897	1.407	d_{C2-O2}	4.325	2.400	1.369
d_{O1-Mn}	1.601	1.701	1.814	d_{O1-Mn}	1.599	1.679	1.817
d_{O2-Mn}	1.599	1.604	1.822	d_{O2-Mn}	1.599	1.609	1.844
$\alpha_{O1-H-Cm}$	169.4	176.5	116.9	$\alpha_{O1-C1-C2}$	76.7	107.3	105.5
$\alpha_{H-Cm-O2}$	44.1	55.1	60.8	$\alpha_{C1-C2-O2}$	119.1	100.1	109.5
$\alpha_{Cm-O2-Mn}$	98.3	100.4	141.7	$\alpha_{C2-O2-Mn}$	99.7	103.2	115.9
$\alpha_{O2-Mn-O1}$	109.2	99.3	101.2	$\alpha_{O2-Mn-O1}$	109.4	100.9	86.1
$\alpha_{Mn-O1-H}$	112.1	108.8	111.5	$\alpha_{Mn-O1-C1}$	134.3	127.2	141.8
$\Phi_{C1-Cm-O2-Mn}$	83.9	−22.9	−21.3	$\Phi_{C1-C2-O2-Mn}$	−12.4	9.3	17.6
2,6-dinitrotoluene C_2-C_3 attack				2,6-dinitrotoluene C_3-C_4 attack			
d_{C2-C3}	1.396	1.457	1.562	d_{C3-C4}	1.391	1.444	1.536
d_{C2-O1}	3.857	2.314	1.363	d_{C3-O1}	3.358	1.725	1.423
d_{C3-O2}	3.315	1.678	1.427	d_{C4-O2}	4.085	2.229	1.433
d_{O1-Mn}	1.599	1.614	1.841	d_{O1-Mn}	1.600	1.689	1.817
d_{O2-Mn}	1.603	1.692	1.807	d_{O2-Mn}	1.599	1.623	1.815
$\alpha_{O1-C2-C3}$	61.2	99.3	110.2	$\alpha_{O1-C3-C4}$	124.3	109.2	107.6
$\alpha_{C2-C3-O2}$	129.6	110.8	107.9	$\alpha_{C3-C4-O2}$	75.7	101.5	108.6
$\alpha_{C3-O2-Mn}$	104.6	124.5	115.5	$\alpha_{C4-O2-Mn}$	111.6	106.8	113.7
$\alpha_{O2-Mn-O1}$	108.9	99.9	86.8	$\alpha_{O2-Mn-O1}$	109.3	99.4	87.7
$\alpha_{Mn-O1-C2}$	116.9	105.4	116.4	$\alpha_{Mn-O1-C3}$	117.9	122.6	114.8
$\Phi_{C2-C3-O2-Mn}$	57.7	2.9	−18.5	$\Phi_{C3-C4-O2-Mn}$	11.8	−7.4	−24.5

Table 7 Charge distribution based on Merz-Singh-Kollman population analysis of selected atoms in modeled oxidation processes of 2,6-dinitrotoluene with permanganate ions (R – reactants, TS – transition states, P – products) at IEFPCM/B3LYP/6-31+G(d,p) theory level

Parameter	*R*	*TS*	*P*	Parameter	*R*	*TS*	*P*
2,6-dinitrotoluene C_m attack				2,6-dinitrotoluene C_1-C_2 attack			
H	0.254	0.403	0.373	C_1	0.045	0.136	0.289
C_m	−0.695	−0.745	−0.048	C_2	0.104	0.330	0.941
O_1	−0.532	−0.650	−0.820	O_1	−0.539	−0.413	−0.618
O_2	−0.532	−0.541	−0.587	O_2	−0.539	−0.473	−0.711
Mn	1.148	1.242	1.201	Mn	1.186	1.087	1.103
O_3	−0.543	−0.533	−0.647	O_3	−0.552	−0.520	−0.585
O_4	−0.536	−0.538	−0.640	O_4	−0.551	−0.523	−0.589
2,6-dinitrotoluene C_2-C_3 attack				2,6-dinitrotoluene C_3-C_4 attack			
C_2	0.070	0.071	0.293	C_3	−0.302	−0.012	0.136
C_3	−0.259	0.221	0.658	C_4	0.023	−0.139	0.399
O_1	−0.525	−0.477	−0.640	O_1	−0.518	−0.450	−0.570
O_2	−0.537	−0.479	−0.694	O_2	−0.533	−0.462	−0.607
Mn	1.161	1.171	1.155	Mn	1.151	1.107	1.070
O_3	−0.542	−0.538	−0.593	O_3	−0.542	−0.542	−0.597
O_4	−0.535	−0.546	−0.606	O_4	−0.543	−0.555	−0.613

possible pathways is given in Fig. 3. In Tables 5, 6, 7, 8, 9, 10 and 11 corresponding energetic parameters and resulting percentage contributions of each alternative reaction in the overall conversion of 2-nitrotoluene and 2,6-nitrotoluene are collected.

As can be seen ring attack probability increases with the increase of nitro groups attached to the aromatic ring. In the case of 2-nitrotoluene the obtained activation Gibbs free energy of methyl group oxidation suggests that reaction proceeds almost exclusively through the methyl group oxidation

Table 8 Bond lengths in aromatic rings (in Å) for HOMA analysis of modeled oxidation processes of 2,6-dinitrotoluene with permanganate ions (R – reactants, TS – transition states, P – products) at IEFPCM/B3LYP/6-31+G(d,p) theory level

Parameter	*R*	*TS*	*P*	Parameter	*R*	*TS*	*P*
2,6-dinitrotoluene C_m attack				2,6-dinitrotoluene C_1-C_2 attack			
C_1-C_2	1.410	1.444	1.412	C_1-C_2	1.409	1.475	1.582
C_2-C_3	1.396	1.394	1.396	C_2-C_3	1.396	1.405	1.508
C_3-C_4	1.391	1.391	1.391	C_3-C_4	1.391	1.379	1.344
C_4-C_5	1.391	1.391	1.391	C_4-C_5	1.391	1.407	1.450
C_5-C_6	1.396	1.395	1.396	C_5-C_6	1.396	1.378	1.349
C_1-C_6	1.408	1.444	1.412	C_1-C_6	1.409	1.484	1.537
HOMA	0.956	0.726	0.944	*HOMA*	0.956	0.243	−2.502
EN	0.029	0.123	0.035	*EN*	0.029	0.286	1.398
GEO	0.015	0.151	0.021	*GEO*	0.015	0.470	2.104
2,6-dinitrotoluene C_2-C_3 attack				2,6-dinitrotoluene C_3-C_4 attack			
Parameter	*R*	*TS*	*P*	Parameter	*R*	*TS*	*P*
C_1-C_2	1.408	1.435	1.527	C_1-C_2	1.409	1.386	1.353
C_2-C_3	1.396	1.457	1.562	C_2-C_3	1.396	1.459	1.517
C_3-C_4	1.392	1.459	1.500	C_3-C_4	1.391	1.444	1.536
C_4-C_5	1.391	1.353	1.339	C_4-C_5	1.391	1.395	1.501
C_5-C_6	1.397	1.433	1.463	C_5-C_6	1.396	1.389	1.342
C_1-C_6	1.409	1.392	1.354	C_1-C_6	1.409	1.437	1.478
HOMA	0.957	0.344	−2.063	*HOMA*	0.956	0.543	−1.695
EN	0.030	0.289	1.245	*EN*	0.029	0.237	1.140
GEO	0.013	0.367	1.819	*GEO*	0.015	0.220	1.556

Table 9 Selected geometric parameters (d – distances in Å, α,Φ – angles in °) of modeled oxidation processes of 2-nitrotoluene with permanganate ions (R – reactants, TS – transition states, P – products) at IEFPCM/B3LYP/6-31+G(d,p) theory level

Parameter	*R*	*TS*	*P*	Parameter	*R*	*TS*	*P*
2-nitrotoluene C_m attack							
d_{Cm-H}	1.095	1.538	2.504				
d_{H-O1}	2.559	1.097	0.967				
d_{Cm-O2}	4.066	2.862	1.412				
d_{O1-Mn}	1.600	1.700	1.816				
d_{O2-Mn}	1.599	1.615	1.824				
$\alpha_{O1-H-Cm}$	166.0	178.5	116.0				
$\alpha_{H-Cm-O2}$	46.6	54.4	81.6				
$\alpha_{Cm-O2-Mn}$	95.8	100.6	127.7				
$\alpha_{O2-Mn-O1}$	109.4	97.9	99.3				
$\alpha_{Mn-O1-H}$	117.1	107.9	115.3				
$\Phi_{C1-Cm-O2-O1}$	−85.0	−94.2	−81.2				
2-nitrotoluene C_1-C_2 attack				2-nitrotoluene C_2-C_3 attack			
d_{C1-C2}	1.412	1.469	1.571	d_{C2-C3}	1.401	1.455	1.549
d_{C1-O1}	4.229	1.729	1.431	d_{C2-O1}	3.597	2.234	1.368
d_{C2-O2}	3.957	2.268	1.345	d_{C3-O2}	4.376	1.718	1.427
d_{O1-Mn}	1.599	1.685	1.808	d_{O1-Mn}	1.599	1.627	1.844
d_{O2-Mn}	1.599	1.623	1.838	d_{O2-Mn}	1.599	1.688	1.810
$\alpha_{O1-C1-C2}$	73.2	108.3	106.3	$\alpha_{O1-C2-C3}$	118.2	100.5	110.2
$\alpha_{C1-C2-O2}$	122.4	100.9	109.6	$\alpha_{C2-C3-O2}$	80.1	110.1	107.4
$\alpha_{C2-O2-Mn}$	104.2	106.9	116.3	$\alpha_{C3-O2-Mn}$	108.3	122.9	115.1
$\alpha_{O2-Mn-O1}$	109.4	98..9	86.4	$\alpha_{O2-Mn-O1}$	109.4	98.9	86.8
$\alpha_{Mn-O1-C1}$	115.4	124.6	116.1	$\alpha_{Mn-O1-C2}$	121.8	107.6	115.3
$\Phi_{C1-C2-O2-O1}$	−8.7	4.8	15.3	$\Phi_{C2-C3-O2-O1}$	−8.3	1.6	21.4
2-nitrotoluene C_3-C_4 attack				2-Nitrotoluene C_4-C_5 attack			
d_{C3-C4}	1.389	1.440	1.532	d_{C4-C5}	1.399	1.447	1.534
d_{C3-O1}	3.931	1.846	1.436	d_{C4-O1}	4.397	2.099	1.425
d_{C4-O2}	4.478	2.055	1.427	d_{C5-O2}	4.347	1.788	1.439
d_{O1-Mn}	1.599	1.671	1.813	d_{O1-Mn}	1.599	1.641	1.819
d_{O2-Mn}	1.599	1.645	1.817	d_{O2-Mn}	1.600	1.68	1.813
$\alpha_{O1-C3-C4}$	121.0	106.9	107.1	$\alpha_{O1-C4-C5}$	109.9	103.3	107.9
$\alpha_{C3-C4-O2}$	121.7	104.6	106.9	$\alpha_{C4-C5-O2}$	86.2	107.9	107.4
$\alpha_{C4-O2-Mn}$	76.2	111.7	113.7	$\alpha_{C5-O2-Mn}$	119.5	120.1	113.4
$\alpha_{O2-Mn-O1}$	115.7	98.0	87.7	$\alpha_{O2-Mn-O1}$	109.5	98.1	87.9
$\alpha_{Mn-O1-C3}$	109.4	118.8	113.2	$\alpha_{Mn-O1-C1}$	105.1	110.3	113.8
$\Phi_{C3-C4-O2-O1}$	−1.5	−0.3	28.0	$\Phi_{C4-C5-O2-O1}$	16.5	−4.9	27.2
2-nitrotoluene C_5-C_6 attack				2-nitrotoluene C_1-C_6 attack			
d_{C5-C6}	1.395	1.443	1.534	d_{C1-C6}	1.405	1.459	1.562
d_{C5-O1}	3.501	1.811	1.432	d_{C1-O1}	3.774	1.833	1.437
d_{C6-O2}	4.128	2.099	1.435	d_{C6-O2}	4.375	2.087	1.426
d_{O1-Mn}	1.601	1.676	1.811	d_{O1-Mn}	1.599	1.671	1.810
d_{O2-Mn}	1.600	1.640	1.816	d_{O2-Mn}	1.600	1.642	1.813
$\alpha_{O1-C5-C6}$	132.9	107.8	106.9	$\alpha_{O1-C1-C6}$	124.1	105.4	106.3
$\alpha_{C5-C6-O2}$	58.6	103.2	108.0	$\alpha_{C1-C6-O2}$	73.4	105.1	107.1
$\alpha_{C6-O2-Mn}$	116.9	110.7	113.4	$\alpha_{C6-O2-Mn}$	115.0	110.6	114.5
$\alpha_{O2-Mn-O1}$	108.9	98.2	87.8	$\alpha_{O2-Mn-O1}$	109.4	98.1	87.4
$\alpha_{Mn-O1-C2}$	160.1	119.6	114.4	$\alpha_{Mn-O1-C1}$	115.0	120.7	115.1
$\Phi_{C5-C6-O2-O1}$	41.6	6.7	26.5	$\Phi_{C1-C6-O2-O1}$	−21.2	−0.2	−27.5

Table 10 Charge distribution based on Merz-Singh-Kollman population analysis of selected atoms in modeled oxidation processes of 2,6-dinitrotoluene with permanganate ions (R – reactants, TS – transition states, P – products) at IEFPCM/B3LYP/6-31+G(d,p) theory level

Parameter	*R*	*TS*	*P*	Parameter	*R*	*TS*	*P*
2-nitrotoluene C_m attack							
H	0.214	0.395	0.474				
C_m	−0.585	−0.824	0.294				
O_1	−0.538	−0.648	−0.915				
O_2	−0.543	−0.574	−0.713				
Mn	1.175	1.212	1.285				
O_3	−0.546	−0.567	−0.671				
O_4	−0.548	−0.570	−0.674				
2-nitrotoluene C_1-C_2 attack				2-nitrotoluene C_2-C_3 attack			
C_1	0.191	0.382	0.472	C_2	0.055	0.136	0.638
C_2	0.126	0.451	1.042	C_3	−0.239	0.141	0.400
O_1	−0.534	−0.524	−0.716	O_1	−0.551	−0.495	−0.631
O_2	−0.528	−0.529	−0.772	O_2	−0.556	−0.485	−0.576
Mn	1.160	1.163	1.165	*Mn*	1.240	1.133	1.110
O_3	−0.550	−0.582	−0.618	O_3	−0.568	−0.570	−0.597
O_4	−0.541	−0.590	−0.622	O_4	−0.561	−0.585	−0.612
2-nitrotoluene C_3-C_4 attack				2-nitrotoluene C_4-C_5 attack			
C_3	−0.271	0.063	0.408	C_4	−0.142	−0.144	0.159
C_4	−0.090	−0.063	0.187	C_5	−0.065	0.319	0.634
O_1	−0.516	−0.484	−0.620	O_1	−0.540	−0.490	−0.626
O_2	−0.531	−0.498	−0.640	O_2	−0.540	−0.512	−0.662
Mn	1.129	1.137	1.130	*Mn*	1.176	1.121	1.074
O_3	−0.534	−0.605	−0.638	O_3	−0.545	−0.590	−0.616
O_4	−0.540	−0.624	−0.642	O_4	−0.549	−0.610	−0.628
2-nitrotoluene C_5-C_6 attack				2-nitrotoluene C_1-C_6 attack			
C_5	−0.127	0.342	0.335	C_1	0.234	0.440	0.780
C_6	−0.193	−0.305	0.414	C_6	−0.200	0.058	0.420
O_1	−0.545	−0.508	−0.671	O_1	−0.520	−0.537	−0.702
O_2	−0.544	−0.474	−0.619	O_2	−0.536	−0.528	−0.713
Mn	1.188	1.093	1.114	*Mn*	1.154	1.162	1.169
O_3	−0.548	−0.579	−0.629	O_3	−0.543	−0.604	−0.644
O_4	−0.547	−0.601	−0.638	O_4	−0.547	−0.626	−0.653

(93 %). In the case of 2,6-dinitrotoluene oxidation the it is only around 68 % with the remaining 32 % proceeding mostly by the attack at the C_3-C_4 bond. This is probably caused by the electron-withdrawing properties of this substituent, which may have negative influence on stabilization of the transition state of methyl group oxidation.

In the case of ring oxidation of nitroaromatics geometries of transition states differ significantly from those obtained for benzene [27] and toluene. Opposite to both C-O bonds (of about 1.95 Å) being nearly equally advanced in the transition state, in the case of toluene nitroderivatives these bonds are quite different; one of them oscillates around 1.7 Å corresponding to bond being nearly half formed (bond order of about 0.45), while the C-O distance remains quite large, around 2.2 Å indicating that the formation of this bond hardly started (bond order of about 0.1). This asymmetry is smaller in the case of 2-nitrotoluene and diminishes slightly with the distance from the nitrosubstituent, with C-O forming bond lengths being about 1.8 and 2.1 Å. This is paralleled by significantly stronger dearomatization occurring in the transition states of ring oxidation of 2-nitro- and 2,6-dinitrotoluene for the attack involving C_1-C_2 and C_2-C_3 bonds. Charge distribution on attacking oxygen atoms follows the same pattern in all reactions of initial slight increase from about −0.55 a.u. to −0.48 a.u. on the transition from the reactants to the transition state and final decrease in the products to average of −0.65 a.u. With the sole exception of the unusually small partial charge on the C_6 atom (−0.31 a.u.) in the reaction proceeding with the attack on the C_5-C_6 bond, atomic charges on the attacked carbon atoms, on the other hand, generally

Table 11 Bond lengths in aromatic rings (in Å) for HOMA analysis of modeled oxidation processes of 2-nitrotoluene with permanganate ions (R – reactants, TS – transition states, P – products) at IEFPCM/B3LYP/6-31+G(d,p) theory level

Parameter	*R*	*TS*	*P*	Parameter	*R*	*TS*	*P*
2-nitrotoluene C_m attack							
C_1-C_2	1.412	1.432	1.406				
C_2-C_3	1.401	1.406	1.401				
C_3-C_4	1.389	1.385	1.390				
C_4-C_5	1.399	1.407	1.399				
C_5-C_6	1.395	1.383	1.394				
C_1-C_6	1.405	1.426	1.403				
HOMA	0.948	0.824	0.962				
EN	0.038	0.088	0.030				
GEO	0.014	0.088	0.008				
2-nitrotoluene C_1-C_2 attack				2-nitrotoluene C_2-C_3 attack			
C_1-C_2	1.412	1.469	1.571	C_1-C_2	1.412	1.438	1.525
C_2-C_3	1.401	1.422	1.509	C_2-C_3	1.401	1.455	1.549
C_3-C_4	1.389	1.369	1.343	C_3-C_4	1.389	1.457	1.506
C_4-C_5	1.399	1.431	1.464	C_4-C_5	1.399	1.361	1.343
C_5-C_6	1.395	1.360	1.342	C_5-C_6	1.395	1.430	1.464
C_1-C_6	1.405	1.473	1.519	C_1-C_6	1.405	1.379	1.348
HOMA	0.948	0.230	−2.230	*HOMA*	0.948	0.385	−1.921
EN	0.038	0.275	1.263	*EN*	0.038	0.264	1.186
GEO	0.014	0.495	1.967	*GEO*	0.014	0.351	1.735
2-nitrotoluene C_3-C_4 attack				2-nitrotoluene C_4-C_5 attack			
C_1-C_2	1.412	1.395	1.370	C_1-C_2	1.412	1.449	1.481
C_2-C_3	1.401	1.449	1.513	C_2-C_3	1.401	1.382	1.344
C_3-C_4	1.389	1.440	1.532	C_3-C_4	1.389	1.412	1.503
C_4-C_5	1.399	1.421	1.502	C_4-C_5	1.399	1.447	1.534
C_5-C_6	1.395	1.376	1.346	C_5-C_6	1.395	1.451	1.508
C_1-C_6	1.405	1.429	1.466	C_1-C_6	1.405	1.369	1.348
HOMA	0.948	0.597	−1.471	*HOMA*	0.948	0.478	−1.625
EN	0.038	0.237	1.151	*EN*	0.038	0.237	1.089
GEO	0.014	0.166	1.320	*GEO*	0.014	0.284	1.537
2-nitrotoluene C_5-C_6 attack				2-nitrotoluene C_1-C_6 attack			
C_1-C_2	1.412	1.395	1.359	C_1-C_2	1.412	1.467	1.527
C_2-C_3	1.401	1.436	1.467	C_2-C_3	1.401	1.382	1.354
C_3-C_4	1.389	1.359	1.340	C_3-C_4	1.389	1.411	1.448
C_4-C_5	1.399	1.449	1.504	C_4-C_5	1.399	1.379	1.347
C_5-C_6	1.395	1.443	1.534	C_5-C_6	1.395	1.416	1.503
C_1-C_6	1.405	1.429	1.527	C_1-C_6	1.405	1.459	1.562
HOMA	0.948	0.501	−1.726	*HOMA*	0.948	0.454	−1.975
EN	0.038	0.240	1.163	*EN*	0.038	0.248	1.221
GEO	0.014	0.259	1.564	*GEO*	0.014	0.298	1.754

increase systematically from the reactant complex to the transition state to product although absolute changes between reactions are very diverse.

As illustrated in Fig. 4 geometries of the transition states of the methyl group oxidation of the considered nitroderivatives are significantly different. In the case of 2,6-dinitrotoluene the structure is almost symmetric and very similar to the one observed in the corresponding toluene oxidation. In the case of 2-nitrotoluene, however, the permanganate anion is rotated about 90 degrees relative to the C_m-C_1 bond. Changes of the dihedral angle Φ throughout the 2,6-dinitrotoluene oxidation molecule are similar to those observed in the case of toluene. In the case of 2-nitrotolune, however, these changes are negligible; the dihedral angle changes from −85° in reactants complex to −94° in the transition state to −81° in the product.

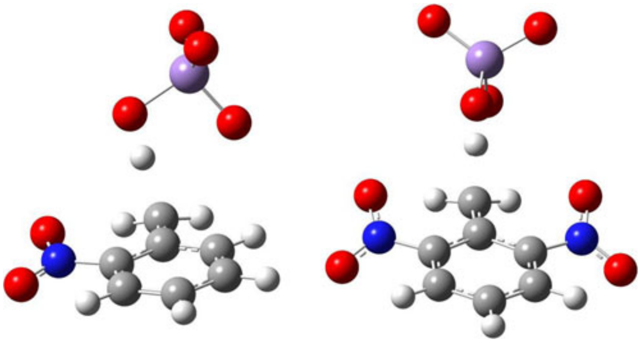

Fig. 4 Transition state structures of methyl group oxidation in modeled oxidation reactions of 2-nitrotoluene and 2,6-dinitrotoluene with permanganate

The length of the breaking C-H bond in 2,6-dinitrotoluene transition state is 1.59 Å, which corresponds to the bond order of 0.24, and is longer than in the case of mono-nitrosubstituted derivative where the corresponding values to 1.54 Å and 0.29, respectively. Analogously, the forming O-H bond in the doubly substituted derivative transition state is 1.08 Å (bond order of 0.73) and is noticeably shorter than in the case of 2-nitrotoluene where the corresponding values are 1.10 Å and 0.69. These results indicate that in both reactions the transition states are late. The overall trend obtained in our studies shows, in agreement with expectations, the increasingly later transition state in the order: toluene, 2-nitrotoluene, 2,6-nitrotoluene. This sequence agrees with the calculated ring dearomatization in the transition state, which increases from toluene to 2-nitrotoluene and 2,6-nitrotoluene with the corresponding HOMA indices equal to 0.91, 0.82 and 0.73, respectively. Partial atomic charges of reacting C···H···O atoms, on the other hand, do not reveal any significant differences; all changes follow the same pattern although the absolute values differ.

Conclusions

We have performed calculations of alternative oxidation pathways of toluene and its *ortho*-substituted nitroderivatives by permanganate anion. Based on the obtained structures of reactants and transition states kinetic isotope effects for each carbon and nitrogen position and subsequently averaged elemental isotopic fractionation have been calculated. These values, compared with experimentally determined ones [5], validated the used theory level. This combination of theoretical and experimental analysis greatly enhances our understanding of oxidative degradation processes of common environmentally important aromatic pollutants.

Our studies show that the preference of the attack position of permanganate anion in oxidation reactions with selected aromatic compounds changes with positions and number of substituents in aromatic ring. On the example of the well studied [8–12] case of toluene oxidation we have shown that the correct preference of methyl group oxidation is predicted when Gibbs free energies from IEFPCM/B3LYP/6-31+G(d,p) calculations, including ZPC and thermal corrections, are used. Furthermore, applying continuum solvent model results in slightly earlier transition states than in the corresponding reaction modeled in gas phase [13]. Obtained charge distribution does not support hydride transfer in toluene oxidation by permanganate. For nitrosubstituted derivatives competitive ring oxidation has been predicted in agreement with the experiment.

From the chemical point of view, ring oxidation reactions proceed via relatively early transition states that become quite unsymmetrical for reactions involving *ortho*-nitrosubstituted derivatives. Transition states for the hydrogen atom abstraction reactions, on the other hand, are late, with C-H bond breaking advanced in about 70 %. All favored reactions are characterized by the Gibbs free energy of activation of about 25 kcal mol^{-1}. Methyl group oxidations are exothermic by about 20 kcal mol^{-1} while ring oxidations are around thermoneutrality.

Acknowledgments This work is supported by the grant PSRP-025/2010 from the Polish-Swiss Research Program. Computing time at the ACK Cyfronet AGH (Krakow, Poland) is gratefully acknowledged.

References

1. Schwarzenbach RP, Egli T, Hofstetter TB, von Gunten U, Wehrli B (2010) Global water pollution and human health. Ann Rev Environ Resour 35:109–136
2. Schwarzenbach R, Gschwend P, Imboden D (2003) Environmental organic chemistry, 2nd edn. Wiley, Hoboken
3. Spain JC (1995) Biodegradation of nitroaromatic compounds. Annu Rev Microbiol 49:523–555
4. Vogt G, Cyrus E, Herklotz I, Schlosser D, Bahr A, Herrmann S, Richnow H-H, Fischer A (2008) Evolution of toluene degradation pathways by two-dimensional stable isotope fractionation. Environ Sci Technol 42:7793–7800
5. Wijker RS, Adamczyk P, Bolotin J, Paneth P, Hofstetter TB (2013) Isotopic analysis of oxidative pollutant degradation pathways exhibiting large H isotope fractionation. Environ Sci Technol 47:13459–13468
6. Wijker RS, Bolotin J, Nishino SF, Spain JC, Hofstetter TB (2013) Using compound-specific isotope analysis to access biodegradation of nitroaromatic explosives in the subsurface. Environ Sci Technol 47:6872–6883
7. Waldemer RH, Tratnyek PG (2006) kinetics of contaminant degradation by permanganate. Environ Sci Technol 40:1055–1061
8. Mayer JM (1998) Hydrogen atom abstraction by metal-oxo complexes: understanding the analogy with organic radical reactions. Acc Chem Res 31:441–450

9. Gardner KA, Kuehnert LL, Mayer JM (1997) Hydrogen atom abstraction by permanganate: oxidations of arylalkanes in organic solvents. Inorg Chem 36:2069–2078
10. Gardner KA, Mayer JA (1995) Understanding C-H bond oxidations: H. and H- transfer in the oxidation of toluene by permanganate. Science 269:1849–1851
11. Thompson MS, Meyer TJ (1982) Kinetics and mechanism of oxidation of aromatic hydrocarbons by Ru(trpy)(bpy)O2+. J Am Chem Soc 104:5070–5076
12. Lee DG, Chen T (1993) Reduction of manganate(VI) by mandelic acid and its significans for development of the general mechanism of oxidation of organic compunds by high-valent transition metal oxides. J Am Chem Soc 115:11231–11326
13. Strassner T, Houk KN (2000) Mechanism of permanganate oxidation of alkanes: hydrogen abstraction and oxygen “rebound”. J Am Chem Soc 122:7821–7822
14. Zhao Y, Schultz NE, Truhlar DG (2006) Design of density functionals by combining the method of constraint satisfaction with parametrization for thermochemistry, thermochemical kinetics and noncovalent interactions. J Chem Theory Comput 2:364–382
15. Zhao Y, Truhlar DG (2008) Density functionals with broad applicability in chemistry. Acc Chem Res 41:157–167
16. Becke AD (1993) Density functional thermochemistry. III. The role of exact exchange. J Chem Phys 98:5648–5652
17. Lee C, Yang W, Parr RG (1988) Development of Coll-Salvetti correlation-energy formula into a functional of the electron density. Phys Rev B 37:785–789
18. Stephens PJ, Devlin FJ, Chabalowski CF, Frisch MJ (1994) Ab initio calculation of vibrational absorption and circular dichroism spectra using density functional force fields. J Chem Phys 98:11623–11627
19. Hariharan PC, Pople JA (1973) The influence of polarization functions on molecular orbital hydrogenation energies. Theor Chim Acta 28:213–222
20. Ditchfield R, Hehre WJ, Pople JA (1971) Self-consistent molecular orbital methods. IX. An extended Gaussian-type basis for molecular-orbital studies of organic molecules. J Chem Phys 54:724–728
21. Francl MM, Pietro WJ, Hehre WJ, Binkley JS, Gordon MS, DeGrees DJ, Pople JA (1982) Self-consistent molecular orbital methods. XXIII. A polarization-type basis set for second-row elements. J Chem Phys 77:3654–3665
22. Clark T, Chandrasekhar J, Spitznagel GW, Von Ragué Schleyer P (1983) Efficient diffuse function-augmented basis sets for anion calculations. III. The 3-21+G basis set for first row elements, lithium to fluoride. J Comp Chem 4:294–301
23. Frisch MJ, Pople JA, Binkley JS (1984) Self-consistent molecular orbital methods. XXV. Supplementary functions for Gaussian basis sets. J Chem Phys 80:3265–3269
24. Miertus S, Scrocco E, Tomasi J (1981) Electrostatic interaction of the solute with a continuum. A direct utilization of the ab initio molecular potentials for the prevision of solvent effects. Chem Phys 55:117
25. Rappe AK, Casewit CJ, Colwell KS, Goddard WA III, Skiff WM (1992) UFF, a full periodic table force field for molecular mechanics and molecular dynamics simulations. J Am Chem Soc 114:10024–10039
26. Adamczyk P, Dybala-Defratyka A, Paneth P (2011) DFT study of trichloroethene reaction with permanganate in aqueous solution. Env Sci Technol 45:3006–3011
27. Adamczyk P, Paneth P (2011) Theoretical evaluation of the isotopic fractionation factors in oxidation reactions of benzene, phenol and chlorophenols. J Mol Model 17:2285–2296
28. Balabanov NB, Peterson KA (2005) Systematically convergent basis sets for the 3d elements Sc-Zn. J Chem Phys 123:064107
29. McWeeny R, Dierksen G (1968) Self-consistent perturbation theory. II. Extension to open shells. J Chem Phys 49:4852–4856
30. Frisch MJ et al (2009) Gaussian 09, Revision A.02. Gaussian, Inc., Wallingford
31. Singh UC, Kollman PA (1984) An approach to computing electrostatic charges for molecules. J Comp Chem 5:129–145
32. Besler BH, Merz KM Jr, Kollman PA (1990) Atomic charges derived from semiempirical methods. J Comp Chem 11:431–439
33. Peng C, Ayala PY, Schlegel HB, Frisch MJ (1996) Using redundant internal coordinates to optimize equilibrium geometries and transition states. J Comp Chem 17:49–56
34. Reed AE, Weinhold F (1983) Natural bond orbital analysis of near-Hartree-Fock water dimer. J Chem Phys 78:4066–4073
35. Fukui K (1970) Formulation of the reaction coordinate. J Phys Chem 74:4161–4163
36. Eyring H, Polanyi M (1931) Über einfache Gasreaktionen. Z Phys Chem Abt B 12:279–311
37. Eyring H (1935) Activated complex in chemical reactions. J Chem Phys 3:107–115
38. Evans MG, Polanyi M (1935) Application of the transition-state method to the calculation of the reaction velocities, especially in solution. Trans Faraday Soc 31:875–894
39. Wigner EP (1932) On the quantum correction for thermodynamic equilibrium. Phys Rev 40:749–759
40. Kruszewski J, Krygowski TM (1972) Definition of aromaticity based on the harmonic oscillator model. Tetrahedron Lett 36:3839–3842
41. Krygowski TM, Cyrański MK (2001) Structural aspects of aromaticity. Chem Rev 101:1385–1419
42. Pauling L (1947) The nature of the interatomic forces in metals. II. Atomic radii and interatomic distances in metals. J Am Chem Soc 69:542–553